Available online at www.sciencedirect.com
SCIENCE DIRECT®
ELSEVIER
International Journal of Solids and Structures 43 (2006) 4795–4809
INTERNATIONAL JOURNAL OF SOLIDS and STRUCTURES
www.elsevier.com/locate/ijsolstr

Dynamic stress intensity factor of the weak/micro-discontinuous interface crack of a FGM coating

Li Yong dong [a,*], Jia Bin [b], Zhang Nan [a], Tang Li qiang [c], Dai Yao [a]

[a] *Division of Engineering Mechanics, Department of Mechanical Engineering, Armored Force Engineering Institute, No. 21, Du Jia Kan, Chang Xin Dian, Beijing 100072, PR China*
[b] *College of Astronautics, Harbin Institute of Technology, Harbin 150001, PR China*
[c] *College of Architectural Engineering, Harbin Engineering University, Harbin 150001, PR China*

Received 7 April 2005
Available online 8 September 2005

Abstract

The concepts and classification are brought forth for the strong-discontinuous interface, the weak-discontinuous interface, the micro-discontinuous interface and the all-continuous interface. The mechanical model is established for the dynamic fracture problem of the weak-discontinuous interface between a FGM coating and a FGM substrate. The Cauchy singular integral equation for the crack is derived by integral transform, and the allocation method is used to get the numerical solution. Analysis of the numerical solution indicates that the weak discontinuity is an important factor affecting the SIFs of the interfacial crack. To reduce the weak discontinuity is beneficial to the decrease of the SIFs. Contrast between the solution of the weak-discontinuous interface and that of the micro-discontinuous one shows that the micro-discontinuity is a kind of connection relation of mechanical property better than the weak discontinuity for the coating–substrate structure. To make the interface be micro-discontinuous is helpful to enhance the capacity of the functionally gradient coating–substrate interface to resist dynamic fracture. The first rank micro-discontinuity is enough to reduce the SIFs notably, however, the higher-rank micro-discontinuous terms, which is equal to or higher than the second rank, have less effect on the SIFs. In addition, the thickness of the coating and the substrate and the applied peel stress are also important factors affecting the dynamic SIFs.

Keywords: Functionally gradient coating; Interfacial crack; Stress intensity factor; Weak-discontinuous interface; Micro-discontinuous interface

* Corresponding author. Tel./fax: +86 10 66719259.
E-mail address: lydbeijing@163.com (Y.d. Li).

0020-7683/$ - see front matter © 2005 Elsevier Ltd. All rights reserved.
doi:10.1016/j.ijsolstr.2005.07.030

1. Introduction

In the research of interface science, the interface fracture mechanics has been an active domain all along. In 1959, Williams first studied the stress fields for a crack along the ideal interface between two dissimilar homogeneous elastic half-planes by the method of series expanding. Afterwards, many researchers carried out fracture analysis for all kinds of ideal interfaces between two elastic–plastic half-planes or two visco-elastic half-planes. It was indicated that the stress fields of the mode I and mode II cracks along the ideally elastic interface have the oscillatory singularity as $r^{-1/2+i\varepsilon}$ where ε is the oscillatory exponent (Williams, 1959; Rice, 1988), and the stress fields of a crack along the elastic–plastic or visco-elastic interface have the similar structure as the famous HRR fields (Wang, 1990; Taher et al., 1994; Tang et al., 2004). Due to the discontinuity of the mechanical properties of the traditional homogeneous bi-material interface, the residual stress level and the stress concentration are high near the interface, which always results in the debonding and fracture of the interface. In order to overcome this shortcoming, the functionally gradient composite, the mechanical properties of which are continuous at the interface, were designed and manufactured these years. After the appearance of the functionally gradient materials (FGMs), the fracture analysis of it became a hotspot in fracture mechanics. It was indicated that the stress fields of a crack in the FGMs has the singularity as $r^{-1/2}$ and the same angular distribution structure as that of a crack in a single elastic material. For the crack-tip fields, the only difference between the FGMs and the homogeneous elastic material is that the continuity of the mechanical properties of the FGMs has remarkable effect on the SIFs (Jin and Noda, 1994). Therefore, an important task of the fracture analysis of FGMs is to study the different effects of the different continuous gradient variations of the mechanical properties on the SIFs. At present, most fracture analysis of FGMs are focused on the fracture mechanical modeling and the solving methods (Delale and Erdogan, 1988; Jin and Batra, 1996a,b; Konda and Erdogan, 1994; Chen and Erdogan, 1996; Wang et al., 2003a,b). The widely used methods for fracture analysis of FGMs can be classified into two categories, one of which is the half-analytical method (Konda and Erdogan, 1994; Chen and Erdogan, 1996) and the other is the numerical method (Kim and Paulino, 2002; Lucia and Paolo, 2004). The half-analytical method is to first derive the singular integral equation by integral transform and then to solve it numerically by the allocation method brought forward by Erdogan. The numerical method is to simulate the fracture problem of the FGMs by a certain finite elements program. There are two kinds of models for the half-analytical method, one of which is the continuous model and the other is the discrete model. The continuous model is to first simulate the variations of the mechanical properties by some continuous function, e.g. the exponential function (Konda and Erdogan, 1994; Chen and Erdogan, 1996), the power function (Wang et al., 1997; Li and Weng, 2001), the hyperbolic function (Wang et al., 2003a) and etc., and then to solve the fracture problem half-analytically. The shortcoming of the continuous model is that every kind of continuous function can only be used to handle a specific continuous gradient variation other than the arbitrary continuous variation of the mechanical properties. Due to the extreme mathematical difficulties arising from the fact that the properties of the FGMs may vary arbitrarily in space, the discrete half-analytical model was put forward. The first discrete half-analytical model is the piecewise multi-layered model (PWML model), in which constant properties in each sub-layer are assumed, and the integral transform is adopted in each sub-layer to carry out the fracture analysis (Qian et al., 1997; Shaw and Leon, 1998). The shortcoming of the PWML model is that the material properties are discontinuous at the sub-interfaces, which does not accord with the reality. To take into account the arbitrary continuous variation of the mechanical properties and at the same time to overcome the disadvantages of the PWML model, Wang et al. (2003b) recently suggested a new multi-layered model (in the following, it is referred to as 'the Wang's multi-layered model') for the fracture analysis of FGMs with properties varying arbitrarily (Huang et al., 2002, 2003, 2004). Based on the fact that an arbitrary curve can be approached by a series of continuous but piecewise linear curves, Wang et al., modeled the FGMs as a multi-layered medium with elastic moduli varying linearly in each sub-layers and continuously at the sub-interfaces and then carry

out the fracture analysis by means of the integral transform. The Wang's multi-layered model is the best discrete half-analytical model up to now.

Most of the current researches on the fracture analysis of the FGMs interface have been devoted to the FGMs interlayer (Delale and Erdogan, 1988; Wang et al., 1997, 2003b; Li and Weng, 2001; Huang et al., 2004) and the interface between the FGM coating and the homogeneous substrate (Chen and Erdogan, 1996; Huang et al., 2002, 2003; Jin and Batra, 1996b; Guo et al., 2004). Due to the continuity of the properties at the interface, the FGMs composites overcome the disadvantages of the traditional homogeneous bi-material interfaces. According to the discontinuity of the mechanical properties and their derivatives at the interface, the bi-material interfaces can be classified into four categories: (a) the strong-discontinuous interface, at which the mechanical properties and their derivatives are all discontinuous, (b) the weak-discontinuous interface, at which the mechanical properties are continuous, but their derivatives are discontinuous, (c) the micro-discontinuous interface, at which the mechanical properties and their lower-rank derivatives are continuous, but their higher-rank derivatives are discontinuous, (d) the all-continuous interface, at which the mechanical properties and their derivatives are all continuous. Because most real composites are always compounded from two different materials, the all-continuous interface does not exist in most real composites. The all-continuous interface can only be regarded as the limit case of the micro-discontinuous interface. From the history of the development of composites, it can be found that nowadays the weak-discontinuous interface is gradually taking place of the strong-discontinuous interface in many important engineering cases, and we can even predict that in the near future the micro-discontinuous interface will necessarily take place of the weak-discontinuous interface in composite engineering. From the strong-discontinuous interface to the weak-discontinuous one, and then to the micro-discontinuous one, this is the law and trend of the development of composite interface. Due to the obscurity of the micro-discontinuity, the effect of it on the fracture behavior of the interface has not been studied. In this paper, the coating and substrate are assumed to be two kinds of FGMs with properties varying differently and connected weak-discontinuously or micro-discontinuously at the interface, which is modeled as an ideal geometrical plane. Based on the fracture mechanical calculation and analysis, the effect of the weak-discontinuity and micro-discontinuity on the dynamic fracture behavior of the coating–substrate interface are discussed.

2. Mechanical model

Illustrated in Fig. 1 is the geometry of an interfacial crack of a FGM coating bonded to a FGM substrate. The shear modulus, the mass density and the thickness of the coating and substrate are denoted by $G_1(y)$, $G_2(y)$, $\rho_1(y)$, $\rho_2(y)$, h_1 and h_2 respectively. It is assumed that the shear modulus and the mass density vary with the coordinate y in the following exponential form

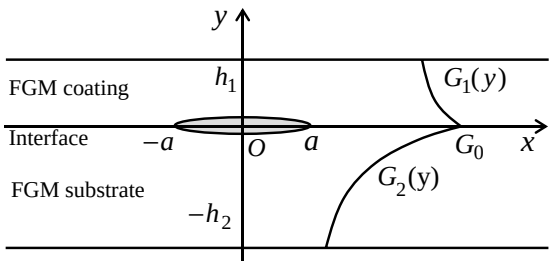

Fig. 1. Interfacial crack of a FGM coating bonded to a FGM substrate.

$$G_1(y) = G_0 e^{\beta_1 y}, \quad \rho_1(y) = \rho_0 e^{\beta_1 y} \tag{1}$$

$$G_2(y) = G_0 e^{\beta_2 y}, \quad \rho_2(y) = \rho_0 e^{\beta_2 y} \tag{2}$$

where G_0 and ρ_0 are the shear modulus and the mass density at the interface. β_1 and β_2 are the non-homogeneity parameters of the coating and substrate respectively.

From Eqs. (1) and (2), it can be found that the material properties are continuous, but their derivatives are discontinuous at the interface, so the interface shown in Fig. 1 is weak-discontinuous. In the previous studies, it was indicated that the influence of the variation of Poisson's ratio on the SIF is rather insignificant (Chen and Erdogan, 1996), so the Poisson's ratios of the coating and the substrate are assumed to be the same in this paper.

It is assumed that the coating–substrate structure in Fig. 1 is loaded at the upper and lower surfaces by dynamic normal stress and shear stress and the crack surface is traction free. As Huang et al. (2003) pointed out, the present problem can be viewed as the superposition of the following two sub-problems: (a) The coating–substrate structure without crack is loaded at the upper and lower surfaces by dynamic normal stress and shear stress, and the stresses induced at the interface are $-\sigma_0(x)H(t)$ and $-\tau_0(x)H(t)$, where $H(t)$ is the Heaviside function. (b) The crack surfaces are loaded by $\sigma_0(x)H(t)$ and $\tau_0(x)H(t)$ and the coating–substrate structure is free of remote loads. Since the problem (a) contributes nothing to the singular fields at the crack-tips, we will pay attention only to problem (b) here, treating $\sigma_0(x)H(t)$ and $\tau_0(x)H(t)$ as known boundary conditions at the crack surfaces. So, the boundary and continuity conditions of problem (b) can be stated as

$$\sigma_{yy}(x, \pm 0, t) = \sigma_0(x)H(t), \quad |x| < a \tag{3}$$

$$\tau_{xy}(x, \pm 0, t) = \tau_0(x)H(t), \quad |x| < a \tag{4}$$

$$\sigma_{yy}(x, +0, t) = \sigma_{yy}(x, -0, t), \quad \tau_{xy}(x, +0, t) = \tau_{xy}(x, -0, t), \qquad |x| < \infty \tag{5}$$

$$u(x, +0, t) = u(x, -0, t), \quad v(x, +0, t) = v(x, -0, t), \qquad |x| > a \tag{6}$$

$$\left.\begin{aligned} &\sigma_{yy}(x, h_1, t) = \tau_{xy}(x, h_1, t) = 0 \\ &\sigma_{yy}(x, -h_2, t) = \tau_{xy}(x, -h_2, t) = 0 \end{aligned}\right\} \tag{7}$$

3. The singular integral equations and the solution

The constitutive relation of the plane problem of the functionally gradient elastic material is as follows:

$$\left.\begin{aligned} \sigma_{xx} &= \frac{G_0 e^{\beta y}}{\kappa - 1}\left[(1+\kappa)\frac{\partial u}{\partial x} + (3-\kappa)\frac{\partial v}{\partial y}\right] \\ \sigma_{yy} &= \frac{G_0 e^{\beta y}}{\kappa - 1}\left[(3-\kappa)\frac{\partial u}{\partial x} + (1+\kappa)\frac{\partial v}{\partial y}\right] \\ \tau_{xy} &= G_0 e^{\beta y}\left(\frac{\partial u}{\partial y} + \frac{\partial v}{\partial x}\right) \end{aligned}\right\} \tag{8}$$

where $\kappa = (3 - \nu)/(1 + \nu)$ for plane stress and $\kappa = 3 - 4\nu$ for plane strain. ν is Poisson's ratio and β is the non-homogeneity parameter of the FGM.

The motion equations of the functionally gradient elastic material are

$$\left.\begin{aligned} \frac{\partial \sigma_{xx}}{\partial x} + \frac{\partial \tau_{yx}}{\partial y} &= \rho_0 e^{\beta y}\frac{\partial^2 u}{\partial t^2} \\ \frac{\partial \sigma_{yy}}{\partial y} + \frac{\partial \tau_{xy}}{\partial x} &= \rho_0 e^{\beta y}\frac{\partial^2 v}{\partial t^2} \end{aligned}\right\} \tag{9}$$

By substituting from Eq. (8) into Eq. (9) and adopting Laplace transform with the initial values of the displacements and their time-derivatives assumed to be zero, i.e. $u(x,y,t=0)=\frac{\partial u(x,y,t)}{\partial t}|_{t=0}=0$ and $v(x,y,t=0)=\frac{\partial v(x,y,t)}{\partial t}|_{t=0}=0$, the governing equations in Laplace domain are obtained as

$$\left.\begin{aligned}&(1+\kappa)\frac{\partial^2\hat{u}}{\partial x^2}+(\kappa-1)\frac{\partial^2\hat{u}}{\partial y^2}+2\frac{\partial^2\hat{v}}{\partial x\partial y}+\beta(\kappa-1)\left(\frac{\partial\hat{u}}{\partial y}+\frac{\partial\hat{v}}{\partial x}\right)=\frac{\rho_0(\kappa-1)p^2}{G_0}\hat{u}\\&(\kappa-1)\frac{\partial^2\hat{v}}{\partial x^2}+(\kappa+1)\frac{\partial^2\hat{v}}{\partial y^2}+2\frac{\partial^2\hat{u}}{\partial x\partial y}+\beta(3-\kappa)\frac{\partial\hat{u}}{\partial x}+\beta(\kappa+1)\frac{\partial\hat{v}}{\partial y}=\frac{\rho_0(\kappa-1)p^2}{G_0}\hat{v}\end{aligned}\right\}\tag{10}$$

where

$$\hat{u}(x,y,p)=\int_0^\infty u(x,y,t)\mathrm{e}^{-pt}\,\mathrm{d}t,\quad \hat{v}(x,y,p)=\int_0^\infty v(x,y,t)\mathrm{e}^{-pt}\,\mathrm{d}t.$$

By using Fourier transforms with respect to x, Eq. (10) can be rewritten as

$$\left.\begin{aligned}&\left[\xi^2(1+\kappa)+\frac{\rho_0(\kappa-1)p^2}{G_0}\right]U+\mathrm{i}\xi\beta(\kappa-1)V+2\mathrm{i}\xi\frac{\mathrm{d}V}{\mathrm{d}y}-\beta(\kappa-1)\frac{\mathrm{d}U}{\mathrm{d}y}-(\kappa-1)\frac{\mathrm{d}^2U}{\mathrm{d}y^2}=0\\&\mathrm{i}\xi\beta(3-\kappa)U+\left[\xi^2(\kappa-1)+\frac{\rho_0(\kappa-1)p^2}{G_0}\right]V+2\mathrm{i}\xi\frac{\mathrm{d}U}{\mathrm{d}y}-\beta(\kappa+1)\frac{\mathrm{d}V}{\mathrm{d}y}-(\kappa+1)\frac{\mathrm{d}^2V}{\mathrm{d}y^2}=0\end{aligned}\right\}\tag{11}$$

where

$$U(\xi,y,p)=\int_{-\infty}^\infty\hat{u}(x,y,p)\mathrm{e}^{\mathrm{i}\xi x}\,\mathrm{d}x\quad\text{and}\quad V(\xi,y,p)=\int_{-\infty}^\infty\hat{v}(x,y,p)\mathrm{e}^{\mathrm{i}\xi x}\,\mathrm{d}x.$$

The solution of Eq. (11) can be expressed as follows:

$$U(\xi,y,p)=\sum_{j=1}^4A_j(\xi,p)\mathrm{e}^{m_jy},\quad V(\xi,y,p)=\sum_{j=1}^4A_j(\xi,p)B_j(\xi,p)\mathrm{e}^{m_jy}\tag{12}$$

where $m_j(\xi,p)$ $(j=1,2,3,4)$ are the roots of the following characteristic equation of Eq. (11)

$$\begin{aligned}&(\kappa^2-1)m^4+2\beta(\kappa^2-1)m^3-\left[(2\xi^2-\beta^2)(\kappa^2-1)+2\kappa(\kappa-1)\rho_0p^2/G_0\right]m^2\\&\quad-\left[2(\kappa^2-1)\xi^2+2\kappa(\kappa-1)\rho_0p^2/G_0\right]\beta m+\beta^2\xi^2(\kappa-1)(3-\kappa)+\xi^4(\kappa^2-1)+2\kappa(\kappa-1)\xi^2\frac{\rho_0p^2}{G_0}\\&\quad+(\kappa-1)^2\frac{\rho_0^2p^4}{G_0^2}=0\end{aligned}\tag{13}$$

$B_j(\xi,p)$ $(j=1,2,3,4)$ can be expressed as

$$B_j=[(\kappa-1)m_j^2+\beta(\kappa-1)m_j-\xi^2(1+\kappa)-(\kappa-1)\rho_0p^2/G_0]/[\mathrm{i}\xi\beta(\kappa-1)+2\mathrm{i}\xi m_j]\tag{14}$$

By using Fourier inversion for Eq. (12), the displacement in Laplace domain can be obtained as

$$\left.\begin{aligned}&\hat{u}(x,y,p)=\frac{1}{2\pi}\int_{-\infty}^\infty\sum_{j=1}^4A_j(\xi,p)\mathrm{e}^{m_jy-\mathrm{i}\xi x}\,\mathrm{d}\xi\\&\hat{v}(x,y,p)=\frac{1}{2\pi}\int_{-\infty}^\infty\sum_{j=1}^4A_j(\xi,p)B_j(\xi,p)\mathrm{e}^{m_jy-\mathrm{i}\xi x}\,\mathrm{d}\xi\end{aligned}\right\}\tag{15}$$

From Eqs. (8) and (15), the stresses in Laplace domain may be expressed as

$$\left.\begin{aligned}\hat{\sigma}_{xx} &= \frac{G_0}{2(\kappa-1)\pi}\int_{-\infty}^{\infty}\sum_{j=1}^{4}\left[(3-\kappa)B_j m_j - \mathrm{i}\xi(1+\kappa)\right]A_j \mathrm{e}^{(m_j+\beta)y-\mathrm{i}\xi x}\,\mathrm{d}\xi \\ \hat{\sigma}_{yy} &= \frac{G_0}{2(\kappa-1)\pi}\int_{-\infty}^{\infty}\sum_{j=1}^{4}\left[(\kappa+1)B_j m_j - \mathrm{i}\xi(3-\kappa)\right]A_j \mathrm{e}^{(m_j+\beta)y-\mathrm{i}\xi x}\,\mathrm{d}\xi \\ \hat{\tau}_{xy} &= \frac{G_0}{2\pi}\int_{-\infty}^{\infty}\sum_{j=1}^{4}(m_j - i\xi B_j)A_j \mathrm{e}^{(m_j+\beta)y-\mathrm{i}\xi x}\,\mathrm{d}\xi\end{aligned}\right\} \tag{16}$$

where

$$\hat{\sigma}_{xx}(x,y,p) = \int_0^{\infty}\sigma_{xx}(x,y,t)\mathrm{e}^{-pt}\,\mathrm{d}t, \quad \hat{\sigma}_{yy}(x,y,p) = \int_0^{\infty}\sigma_{yy}(x,y,t)\mathrm{e}^{-pt}\,\mathrm{d}t,$$
$$\hat{\tau}_{xy}(x,y,p) = \int_0^{\infty}\tau_{xy}(x,y,t)\mathrm{e}^{-pt}\,\mathrm{d}t$$

By substituting β in Eqs. (8)–(16) with β_k ($k = 1, 2$), the corresponding equations of the coating and substrate in Fig. 1 can be obtained respectively.

From Eqs. (16), (7) and (5), the following relations can be got

$$\left.\begin{aligned}A_3|_{y>0} &= d_{11}A_1|_{y>0} + d_{12}A_2|_{y>0}, \quad A_4|_{y>0} = d_{21}A_1|_{y>0} + d_{22}A_2|_{y>0} \\ A_1|_{y<0} &= d_{31}A_1|_{y>0} + d_{32}A_2|_{y>0}, \quad A_2|_{y<0} = d_{41}A_1|_{y>0} + d_{42}A_2|_{y>0} \\ A_3|_{y<0} &= d_{51}A_1|_{y>0} + d_{52}A_2|_{y>0}, \quad A_4|_{y<0} = d_{61}A_1|_{y>0} + d_{62}A_2|_{y>0}\end{aligned}\right\} \tag{17}$$

where d_{ij} ($i = 1,2,3,4,5,6$ and $j = 1,2$) are listed in Appendix A.

From Eq. (17), it can be found that if $A_1(\xi)|_{y>0}$ and $A_2(\xi)|_{y>0}$ are got, then the whole problem can be solved. Therefore, two unknown dislocation density functions are introduced as follows:

$$\left.\begin{aligned}g_1(x,p) &= \frac{\partial\hat{u}(x,+0,p)}{\partial x} - \frac{\partial\hat{u}(x,-0,p)}{\partial x} \\ g_2(x,p) &= \frac{\partial\hat{v}(x,+0,p)}{\partial x} - \frac{\partial\hat{v}(x,-0,p)}{\partial x}\end{aligned}\right\} \tag{18}$$

By using Eq. (18), the continuity condition Eq. (6) can be rewritten as

$$g_1(x,p) = g_2(x,p) = 0, \quad |x| > a \tag{19}$$

From Eqs. (12), (18) and (19), the following relations can be obtained:

$$\left.\begin{aligned}\frac{\mathrm{i}}{\xi}\int_{-a}^{a} g_1(x,p)\mathrm{e}^{\mathrm{i}\xi x}\,\mathrm{d}x &= e_{11}A_1|_{y>0} + e_{12}A_2|_{y>0} \\ \frac{\mathrm{i}}{\xi}\int_{-a}^{a} g_2(x,p)\mathrm{e}^{\mathrm{i}\xi x}\,\mathrm{d}x &= e_{21}A_1|_{y>0} + e_{22}A_2|_{y>0}\end{aligned}\right\} \tag{20}$$

where e_{ij} ($i = 1, 2$ and $j = 1, 2$) are listed in Appendix A.

Using Laplace transform for Eqs. (3) and (4), we have

$$\left.\begin{aligned}\hat{\sigma}_{yy}(x,\pm 0,p) &= \sigma_0(x)/p, \quad |x| < a \\ \hat{\tau}_{xy}(x,\pm 0,p) &= \tau_0(x)/p, \quad |x| < a\end{aligned}\right\} \tag{21}$$

Let $y \to +0$, from Eqs. (21), (20), (17) and (16), the following integral equations can be obtained

$$\left.\begin{aligned} &\frac{1}{\pi}\int_{-a}^{a}[R_{11}(x,s)g_1(s,p)+R_{12}(x,s)g_2(s,p)]\,\mathrm{d}s=\frac{2(\kappa-1)\sigma_0(x)}{pG_0}, \quad |x|<a\\ &\frac{1}{\pi}\int_{-a}^{a}[R_{21}(x,s)g_1(s,p)+R_{22}(x,s)g_2(s,p)]\,\mathrm{d}s=\frac{2\tau_0(x)}{pG_0}, \quad |x|<a \end{aligned}\right\} \tag{22}$$

where

$$R_{11}(x,s)=\int_{-\infty}^{\infty}H_{11}\mathrm{e}^{\mathrm{i}\xi(s-x)}\,\mathrm{d}\xi, \quad R_{12}(x,s)=\int_{-\infty}^{\infty}H_{12}\mathrm{e}^{\mathrm{i}\xi(s-x)}\,\mathrm{d}\xi,$$
$$R_{21}(x,s)=\int_{-\infty}^{\infty}H_{21}\mathrm{e}^{\mathrm{i}\xi(s-x)}\,\mathrm{d}\xi, \quad R_{22}(x,s)=\int_{-\infty}^{\infty}H_{22}\mathrm{e}^{\mathrm{i}\xi(s-x)}\,\mathrm{d}\xi$$

H_{ij} $(i=1,2$ and $j=1,2)$are listed in Appendix A.

When $\xi \to \infty$, the asymptotic values of H_{ij} $(i, j = 1, 2)$ are

$$\lim_{\xi\to\infty}H_{11}=\lim_{\xi\to\infty}H_{22}=0 \quad \text{and} \quad \lim_{\xi\to\infty}H_{12}=\lim_{\xi\to\infty}H_{21}=\frac{1}{2\mathrm{i}}\operatorname{sgn}(\xi)$$

From the formula of Riemann–Lebesgue $\frac{1}{2\mathrm{i}}\int_{-\infty}^{+\infty}\operatorname{sgn}(\xi)\mathrm{e}^{\mathrm{i}\xi(s-x)}\,\mathrm{d}\xi=\frac{1}{s-x}$, it can be found that when $\xi \to \infty$, only the asymptotic values of H_{12} and H_{21} will lead to unbounded integrals. By adding and subtracting $\lim_{\xi\to\infty}H_{ij}$ to and from H_{ij} $(i, j = 1, 2)$, then the following singular integral equations with Cauchy kernels can be obtained

$$\left.\begin{aligned} &\frac{1}{\pi}\int_{-a}^{a}\left[\frac{g_2(s,p)}{s-x}+k_{11}(x,s)g_1(s,p)+k_{12}(x,s)g_2(s,p)\right]\mathrm{d}s=\frac{2(\kappa-1)\sigma_0(x)}{pG_0}, \quad |x|<a\\ &\frac{1}{\pi}\int_{-a}^{a}\left[\frac{g_1(s,p)}{s-x}+k_{21}(x,s)g_1(s,p)+k_{22}(x,s)g_2(s,p)\right]\mathrm{d}s=\frac{2\tau_0(x)}{pG_0}, \quad |x|<a \end{aligned}\right\} \tag{23}$$

where

$$k_{11}(x,s)=R_{11}(x,s), \quad k_{12}(x,s)=\int_{-\infty}^{\infty}(H_{12}-\lim_{\xi\to\infty}H_{12})\mathrm{e}^{\mathrm{i}\xi(s-x)}\,\mathrm{d}\xi,$$
$$k_{22}(x,s)=R_{22}(x,s), \quad k_{21}(x,s)=\int_{-\infty}^{\infty}(H_{21}-\lim_{\xi\to\infty}H_{21})\mathrm{e}^{\mathrm{i}\xi(s-x)}\,\mathrm{d}\xi$$

By introducing the linear transforms $\tilde{s}=s/a\in(-1,1)$ and $\tilde{x}=x/a\in(-1,1)$, the Cauchy singular Eqs. (23) can be rewritten as

$$\left.\begin{aligned} &\frac{1}{\pi}\int_{-1}^{1}\left[\frac{\tilde{g}_2(\tilde{s},p)}{\tilde{s}-\tilde{x}}+a\tilde{k}_{11}(\tilde{x},\tilde{s})\tilde{g}_1(\tilde{s},p)+a\tilde{k}_{12}(\tilde{x},\tilde{s})\tilde{g}_2(\tilde{s},p)\right]\mathrm{d}\tilde{s}=\frac{2(\kappa-1)\tilde{\sigma}_0(a\tilde{x})}{pG_0}\\ &\frac{1}{\pi}\int_{-1}^{1}\left[\frac{\tilde{g}_1(\tilde{s},p)}{\tilde{s}-\tilde{x}}+a\tilde{k}_{21}(\tilde{x},\tilde{s})\tilde{g}_1(\tilde{s},p)+a\tilde{k}_{22}(\tilde{x},\tilde{s})\tilde{g}_2(\tilde{s},p)\right]\mathrm{d}\tilde{s}=\frac{2\tilde{\tau}_0(a\tilde{x})}{pG_0} \end{aligned}\right\} \tag{24}$$

where

$$\tilde{g}_1(\tilde{s},p)=g_1(a\tilde{s},p), \quad \tilde{g}_2(\tilde{s},p)=g_2(a\tilde{s},p), \quad \tilde{\sigma}_0(\tilde{x})=\sigma_0(a\tilde{x}), \quad \tilde{\tau}_0(\tilde{x})=\tau_0(a\tilde{x}),$$
$$\tilde{k}_{ij}(\tilde{x},\tilde{s})=k_{ij}(a\tilde{x},a\tilde{s}), \ i,j=1,2.$$

The Cauchy singular equation (24) can be solved with the numerical method proposed by Erdogan and Gupta (1972). Due to the fact that the basic solution of the singular integral in Eq. (24) is $\omega(\tilde{s})=1/\sqrt{1-\tilde{s}^2}$,

the two unknowns $\tilde{g}_1(\tilde{s},p)$ and $\tilde{g}_2(\tilde{s},p)$ and the stresses at the crack-tip in Fig. 1 would have the conventional square-root singularity (Chen and Erdogan, 1996). Because $1/\sqrt{1-\tilde{s}^2}$ is the weight function of the first kind of Chebyshev polynomial, the unknowns $\tilde{g}_1(\tilde{s},p)$ and $\tilde{g}_2(\tilde{s},p)$ can be expanded as series in terms of Chebyshev polynomials, which are always truncated in calculation as follows:

$$\tilde{g}_1(\tilde{s},p)=\frac{1}{\sqrt{1-\tilde{s}^2}}\frac{1}{p}\sum_{j=0}^{n}C_jT_j(\tilde{s}),\quad \tilde{g}_2(\tilde{s},p)=\frac{1}{\sqrt{1-\tilde{s}^2}}\frac{1}{p}\sum_{j=0}^{n}D_jT_j(\tilde{s}) \tag{25}$$

where C_j and D_j are unknowns, and $T_j(\tilde{s})=\cos(j\arccos\tilde{s})$ are the Chebyshev polynomials of the first kind, which are related to the Chebyshev polynomials of the second kind as follows:

$$\frac{1}{\pi}\int_{-1}^{1}\frac{T_j(\tilde{s})}{(\tilde{s}-\tilde{x})\sqrt{1-\tilde{s}^2}}\,\mathrm{d}\tilde{s}=\begin{cases}0, & j=0,\ |\tilde{x}|<1\\ U_{j-1}(\tilde{x}), & j\geqslant 1,\ |\tilde{x}|<1\end{cases} \tag{26}$$

where $U_{j-1}(\tilde{x})=\frac{1}{\sqrt{1-\tilde{x}^2}}\sin(j\arccos\tilde{x})$ is the Chebyshev polynomials of the second kind.

By using Eqs. (25) and (26), the Cauchy singular equation (24) may be reduced to a system of algebra equations

$$\left.\begin{aligned}&\sum\nolimits_{r=1}^{M}\left\{\left[\frac{1}{\tilde{s}_r-\tilde{x}_q}+a\tilde{k}_{12}(\tilde{x}_q,\tilde{s}_r)\right]\tilde{g}_2(\tilde{s}_r,p)+a\tilde{k}_{11}(\tilde{x}_q,\tilde{s}_r)\tilde{g}_1(\tilde{s}_r,p)\right\}\sqrt{1-\tilde{s}_r^2}=\frac{2(\kappa-1)\tilde{\sigma}_0(\tilde{x}_q)M}{G_0}\\ &\sum\nolimits_{r=1}^{M}\left\{\left[\frac{1}{\tilde{s}_r-\tilde{x}_q}+a\tilde{k}_{21}(\tilde{x}_q,\tilde{s}_r)\right]\tilde{g}_1(\tilde{s}_r,p)+a\tilde{k}_{22}(\tilde{x}_q,\tilde{s}_r)\tilde{g}_2(\tilde{s}_r,p)\right\}\sqrt{1-\tilde{s}_r^2}=\frac{2\tilde{\tau}_0(\tilde{x}_q)M}{G_0}\end{aligned}\right\} \tag{27}$$

where $\tilde{s}_r$ and $\tilde{x}_q$ are the roots of the first and second kinds of Chebyshev polynomials respectively

$$\left.\begin{aligned}&\tilde{s}_r=\cos\frac{(2r-1)\pi}{2M},\quad (r=1,2,\ldots,M)\\ &\tilde{x}_q=\cos\frac{q\pi}{M},\quad (q=1,2,\ldots,M-1)\end{aligned}\right\} \tag{28}$$

Eq. (27) should be solved under the following single-valuedness conditions

$$\left.\begin{aligned}&\int_{-1}^{1}\tilde{g}_1(\tilde{s},p)\,\mathrm{d}\tilde{s}=0\\ &\int_{-1}^{1}\tilde{g}_2(\tilde{s},p)\,\mathrm{d}\tilde{s}=0\end{aligned}\right\} \tag{29}$$

By discretizing the integrals in Eq. (29), the following system of algebra equations can be obtained

$$\left.\begin{aligned}&\sum\nolimits_{r=1}^{M}\tilde{g}_1(\tilde{s}_r,p)\sqrt{1-\tilde{s}_r^2}=0\\ &\sum\nolimits_{r=1}^{M}\tilde{g}_2(\tilde{s}_r,p)\sqrt{1-\tilde{s}_r^2}=0\end{aligned}\right\} \tag{30}$$

From Eqs. (27) and (30), all of the unknowns can be determined numerically.

4. Numerical result and discussion

Due to the asymmetry of the mechanical properties with respect to the interface in Fig. 1, the crack-tip will be always in mixed mode. So, in general, the mode I and II SIFs, K_{I} and K_{II}, will not be zero at the same time. Because the interfacial crack in Fig. 1 is perpendicular to the gradient direction of the mechanical properties, the SIFs at the left and right tip will be the same. Based on the numerical solution of Eqs. (27) and (30), the mode I and II SIFs in Laplace domain can be defined as

$$\left.\begin{aligned}\widehat{K}_{\mathrm{I}}(a,p) &= \lim_{x\to a^+}\sqrt{2\pi(x-a)}\hat{\sigma}_{yy}(x,0,p)\\ \widehat{K}_{\mathrm{II}}(a,p) &= \lim_{x\to a^+}\sqrt{2\pi(x-a)}\hat{\tau}_{xy}(x,0,p)\end{aligned}\right\} \tag{31}$$

By using the following property of the first kind of Chebyshev polynomials $T_j(\tilde{s})$

$$\frac{1}{\pi}\int_{-1}^{1}\frac{T_j(\tilde{s})}{(\tilde{s}-\tilde{x})\sqrt{1-\tilde{s}^2}}\,\mathrm{d}\tilde{s} = -\frac{\mathrm{sgn}(\tilde{x})}{\sqrt{\tilde{x}^2-1}}\left[\tilde{x}-\mathrm{sgn}(\tilde{x})\sqrt{\tilde{x}^2-1}\right]^n, \quad j\geqslant 0,\ |\tilde{x}|>1$$

then the definitions in Eq. (31) can be rewritten as

$$\left.\begin{aligned}\widehat{K}_{\mathrm{I}}(a,p) &= -\frac{2G_0}{p(\kappa+1)}\sqrt{\pi a}\sum_{j=0}^{n}D_j\\ \widehat{K}_{\mathrm{II}}(a,p) &= -\frac{2G_0}{p(\kappa+1)}\sqrt{\pi a}\sum_{j=0}^{n}C_j\end{aligned}\right\} \tag{32}$$

By using Laplace numerical inversion proposed by Miller and Guy (1966), the mode I and II SIFs, $K_{\mathrm{I}}(a,t)$ and $K_{\mathrm{II}}(a,t)$, in the time domain can be obtained from Eq. (32). Shown in Figs. 2–5 are the dynamic SIFs for plane strain with the crack surfaces loaded by the step stresses $\sigma_0 H(t)$ and $\tau_0 H(t)$. In these figures, $c_0=\sqrt{G_0/\rho_0}$ is the shear wave velocity at the interface, $c_0 t/a$ is the non-dimensional time, and the stress intensity factors are normalized as follows:

$$\overline{K_{\mathrm{I}}}(a,t)=\frac{K_{\mathrm{I}}(a,t)}{\sigma_0\sqrt{\pi a}}, \quad \overline{K_{\mathrm{II}}}(a,t)=\frac{K_{\mathrm{II}}(a,t)}{\sigma_0\sqrt{\pi a}} \tag{33}$$

Figs. 2 and 3 show the effect of the thickness of the coating and substrate on the dynamic SIFs. It is indicated that with the thickness of the coating and substrate increasing the peak values of the dynamic SIFs decrease and the attenuation velocity of the dynamic SIFs increases. So a conclusion can be drawn that thicker coating and substrate are beneficial to the reduction of the dynamic SIFs of the interfacial crack and to the enhancement of the capacity of the coating–substrate structure to resist dynamic fracture.

Figs. 2 and 3 also show the effect of the loading mode on the dynamic SIFs. The following three kinds of loading modes have been taken into consideration respectively: (a) the coating–substrate structure being loaded only by the peel stress σ_0; (b) the coating–substrate structure being loaded only by the shear stress τ_0; (c) the coating–substrate structure being loaded by both the peel stress σ_0 and the shear stress τ_0. It is indicated that, in all the three kinds of loading modes, both $\overline{K_{\mathrm{I}}}(a,t)$ and $\overline{K_{\mathrm{II}}}(a,t)$ are non-zero, and the peel stress has more important effects on the dynamic SIFs than the shear stress. So the peel stress is a more important factor than the shear stress resulting in the failure of the coating–substrate interface.

Fig. 4 shows the effects of the ratio of the nonhomogeneity parameters of the coating and substrate on the dynamic SIFs. It can be found that the peak values of the dynamic SIFs decrease notably with decreasing β_1/β_2. When $\beta_1/\beta_2=1$, the peak value of the dynamic SIF reaches the minimum. Therefore, to diminish the difference between β_1 and β_2 will also be beneficial to the reduction of the dynamic SIFs of the interfacial crack and to the enhancement of the capacity of the coating–substrate structure to endure dynamic loads. When $\beta_1/\beta_2\neq 1$, the coating–substrate interface will be weak-discontinuous. The greater the difference between β_1 and β_2 is, the more remarkable the weak-discontinuity of the interface and the higher the peak values of the dynamic SIFs. So, the weak-discontinuity of the coating–substrate interface is an important factor affecting the dynamic SIFs of the interfacial crack. When $\beta_1/\beta_2=1$, the coating–substrate interface will be all-continuous. Under the same condition, the dynamic SIF of the all-continuous interface is always smaller than that of the weak-discontinuous one.

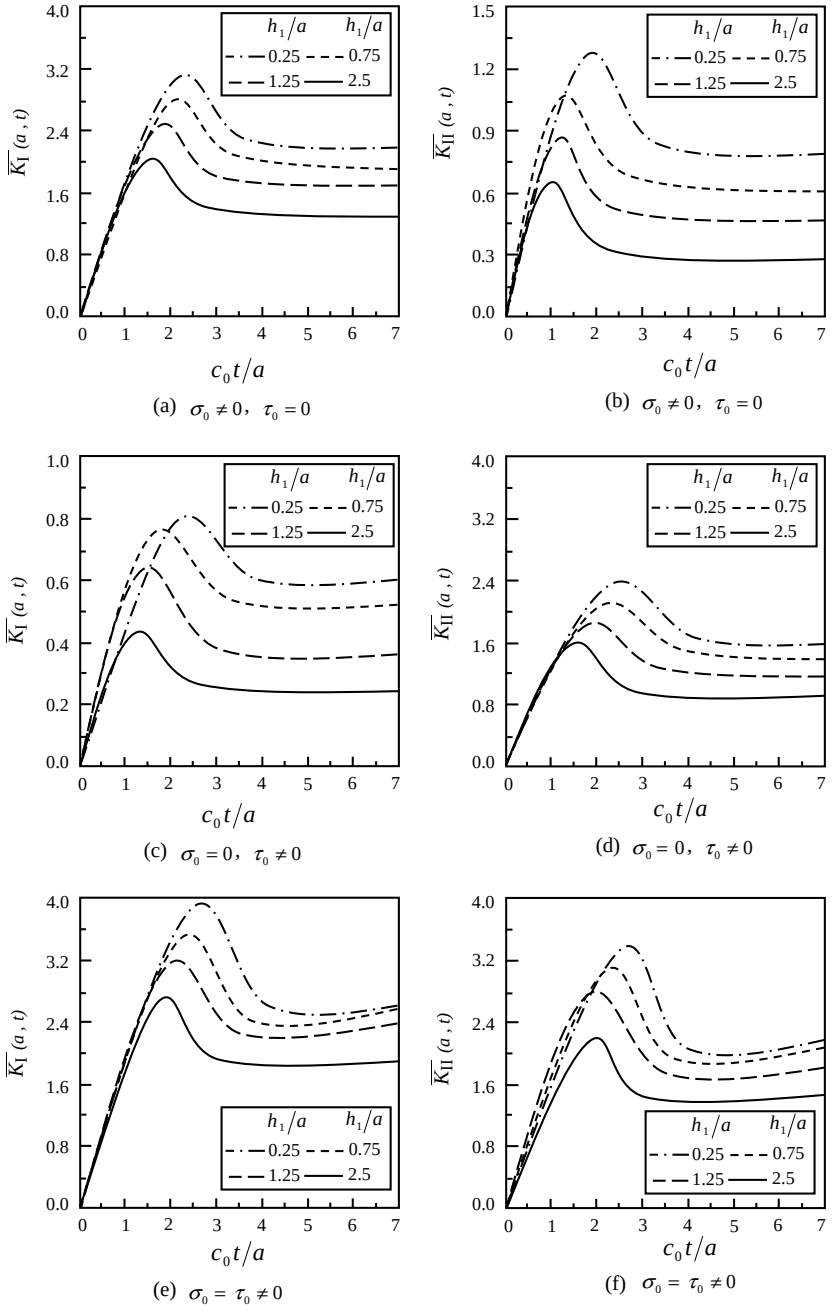

Fig. 2. The effect of the coating thickness on the dynamic SIFs ($h_2/a = 50$, $\beta_1/\beta_2 = 2$).

In engineering, it is impossible and unnecessary to make all the FGMs coating–substrate interface all-continuous. One effective method to diminish the peak values of the dynamic SIFs is to reduce the weak-discontinuity of the interface, i.e. as mentioned above, to reduce the difference between the non-

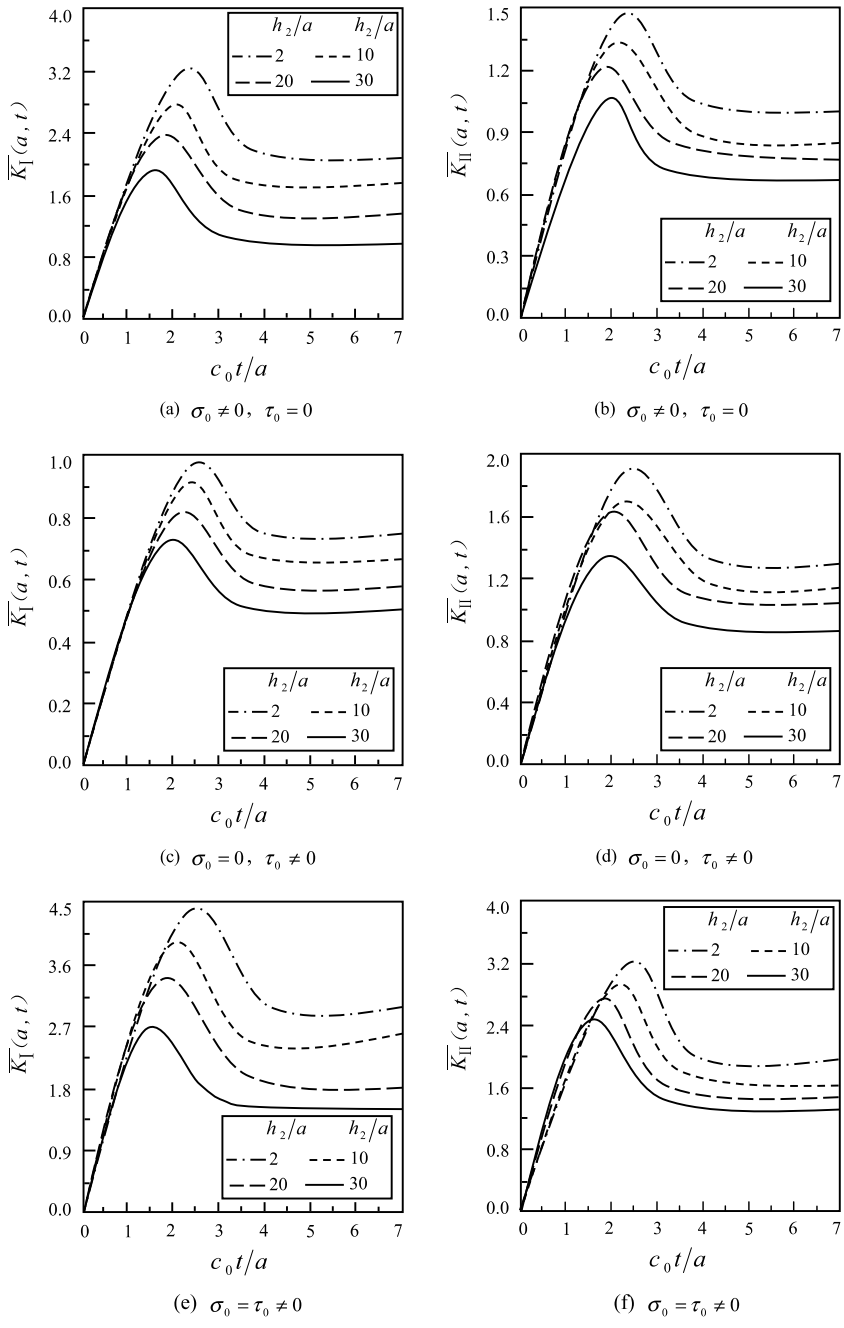

Fig. 3. The effect of the substrate thickness on the dynamic SIFs ($h_1/a = 2$, $\beta_1/\beta_2 = 2$).

homogeneity parameters β_1 and β_2, another possible method is to seek a compromise between the weak-discontinuity and the all-continuity, that is, to make the FGMs coating–substrate interface be micro-discontinuous. For example, if the mechanical property of the substrate is made to be the lower-rank terms

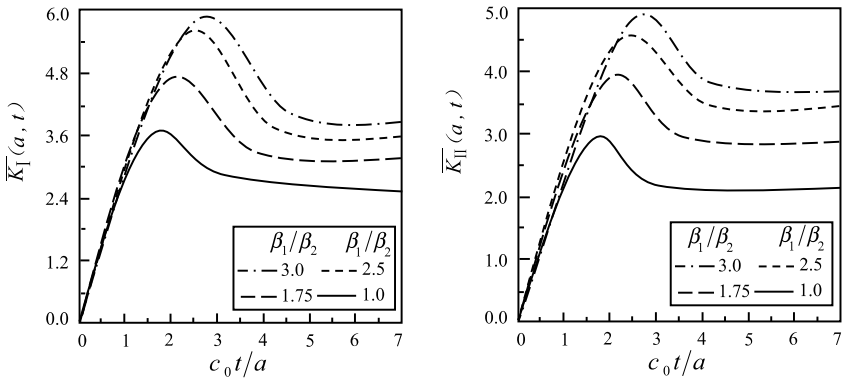

(a) the mode- Ⅰ SIFs (b) the mode-Ⅱ SIFs

Fig. 4. The effect of the ratio between the two nonhomogenity parameters on the SIFs ($h_1/a = 1$, $h_2/a = 50$, $\sigma_0 = \tau_0 \neq 0$).

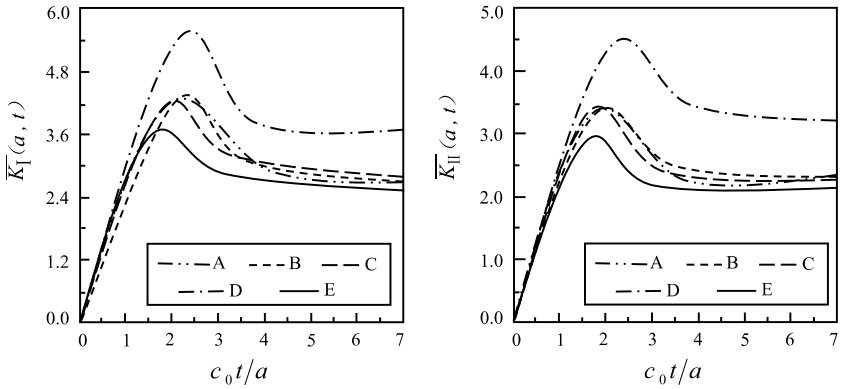

(a) the mode- Ⅰ SIFs (b) the mode-Ⅱ SIFs

Fig. 5. The effect of different types of discontinuity on the SIFs ($h_1/a = 1$, $h_2/a = 50$, $\sigma_0 = \tau_0 \neq 0$).

of the Taylor series of that of the coating at the interface, the coating–substrate interface will become micro-discontinuous. In order to study the effect of the micro-discontinuity on the dynamic SIFs, here the shear modulus $G_2(y)$ and the mass density $\rho_2(y)$ of the substrate are assumed to be the lower-rank terms of the Taylor series of $G_1(y)$ and $\rho_1(y)$ of the coating at the interface, and the dynamic SIFs of the coating–substrate interfacial crack loaded by step stresses $\sigma_0 H(t)$ and $\tau_0 H(t)$ are simulated by the finite elements method for the following three cases.

Case A (i.e. the first-rank micro-discontinuous interface):

$$\left.\begin{aligned} G_1(y) &= G_0 \mathrm{e}^{\beta_1 y}, \quad G_2(y) = G_0 + G_0\beta_1 y \\ \rho_1(y) &= \rho_0 \mathrm{e}^{\beta_1 y}, \quad \rho_2(y) = \rho_0 + \rho_0\beta_1 y \end{aligned}\right\} \tag{34}$$

Case B (i.e. the second-rank micro-discontinuous interface):

$$\left.\begin{aligned} G_1(y) &= G_0 \mathrm{e}^{\beta_1 y}, \quad G_2(y) = G_0 + G_0\beta_1 y + \frac{1}{2}G_0\beta_1^2 y^2 \\ \rho_1(y) &= \rho_0 \mathrm{e}^{\beta_1 y}, \quad \rho_2(y) = \rho_0 + \rho_0\beta_1 y + \frac{1}{2}\rho_0\beta_1^2 y^2 \end{aligned}\right\} \tag{35}$$

Case C (i.e. the third-rank micro-discontinuous interface):

$$\left.\begin{aligned} G_1(y) &= G_0 e^{\beta_1 y}, \quad G_2(y) = G_0 + G_0\beta_1 y + \frac{1}{2}G_0\beta_1^2 y^2 + \frac{1}{6}G_0\beta_1^3 y^3 \\ \rho_1(y) &= \rho_0 e^{\beta_1 y}, \quad \rho_2(y) = \rho_0 + \rho_0\beta_1 y + \frac{1}{2}\rho_0\beta_1^2 y^2 + \frac{1}{6}\rho_0\beta_1^3 y^3 \end{aligned}\right\} \tag{36}$$

where the rank of the micro-discontinuity refers to the rank of the polynomial got from the Taylor series of the mechanical property.

The dynamic SIFs of the micro-discontinuous interface are contrasted with those of the weak-discontinuous and all-continuous interfaces in Fig. 5, where curve A denotes the first-rank micro-discontinuous case in Eq. (34), curve B denotes the second-rank micro-discontinuous case in Eq. (35), curve C denotes the third-rank micro-discontinuous case in Eq. (36), curve D denotes the weak-discontinuous case with $\beta_1/\beta_2 = 2$, and curve E denotes the all-continuous case (i.e. $\beta_1/\beta_2 = 1$). It is indicated that the dynamic SIFs corresponding to the micro-discontinuous cases are remarkably lower than that of the weak-discontinuous case and are relatively close to that corresponding to the all-continuous case. The difference between the dynamic SIFs corresponding to the first, second and third rank micro-discontinuous cases is very small. Therefore, when the all-continuous case is impossible in engineering reality, the micro-discontinuous case may always meet the demand of high capacity of the interface between the FGMs coating and substrate to resist dynamic fracture. Because the first rank micro-discontinuity is enough to reduce the dynamic SIFs notably, it is not necessary to manufacture FGMs coating–substrate interface with higher rank micro-discontinuity in engineering.

5. Conclusions

(1) To increase the thickness of the coating and substrate is beneficial to the reduction of the peak value of the dynamic SIFs of the interfacial crack, that is, to the enhancement of the capacity of the FGMs coating–substrate structure to resist dynamic fracture.

(2) The peel stress is a more important factor than the shear stress resulting in the failure of the coating–substrate interface. To reduce the applied peel stress is helpful to the reduction of interface failure.

(3) The weak-discontinuity of the FGMs coating–substrate interface is an important factor affecting the dynamic SIFs of the interfacial crack. The greater the difference between the nonhomogeneity parameters of the FGMs coating and substrate is, the more remarkable the weak-discontinuity of the interface and the higher the peak values of the dynamic SIFs.

(4) If the mechanical property of the substrate is made to be the lower-rank terms of the Taylor series of that of the coating at the interface, the coating–substrate interface will become micro-discontinuous. Under the same condition, the dynamic SIFs corresponding to the micro-discontinuous cases are remarkably lower than those of the weak-discontinuous cases. The first-rank micro-discontinuity is always enough to reduce the dynamic SIFs notably, and the higher-rank micro-discontinuous terms have very small effect on the dynamic SIFs. To reduce the weak-discontinuity of the interface or to make the interface be micro-discontinuous is beneficial to the enhancement of the capacity of the interface to resist dynamic fracture.

Acknowledgement

This work was supported by the Natural Science Foundation of PR China under the grant No. 90305023.

Appendix A

$$d_{11}=\frac{(c_{21}c_{14}c_{34}c_{43}c_{56}c_{65}-c_{11}c_{24}c_{31}c_{42}c_{57}c_{68})}{c_{13}c_{24}c_{31}c_{42}c_{57}c_{68}-c_{14}c_{23}c_{34}c_{43}c_{56}c_{65}};\quad d_{12}=\frac{(c_{22}c_{14}c_{34}c_{43}c_{56}c_{65}-c_{12}c_{24}c_{31}c_{42}c_{57}c_{68})}{c_{13}c_{24}c_{31}c_{42}c_{57}c_{68}-c_{14}c_{23}c_{34}c_{43}c_{56}c_{65}}$$

$$d_{21}=\frac{(c_{11}c_{23}c_{34}c_{43}c_{56}c_{65}-c_{21}c_{13}c_{31}c_{42}c_{57}c_{68})}{c_{13}c_{24}c_{31}c_{42}c_{57}c_{68}-c_{14}c_{23}c_{34}c_{43}c_{56}c_{65}};\quad d_{22}=\frac{(c_{12}c_{23}c_{34}c_{43}c_{56}c_{65}-c_{22}c_{13}c_{31}c_{42}c_{57}c_{68})}{c_{13}c_{24}c_{31}c_{42}c_{57}c_{68}-c_{14}c_{23}c_{34}c_{43}c_{56}c_{65}}$$

$$d_{31}=\frac{(c_{21}c_{14}c_{32}c_{43}c_{58}c_{63}-c_{61}c_{34}c_{43}c_{56}c_{14}c_{23})}{c_{13}c_{24}c_{31}c_{42}c_{57}c_{68}-c_{14}c_{23}c_{34}c_{43}c_{56}c_{65}};\quad d_{32}=\frac{(c_{22}c_{14}c_{32}c_{43}c_{58}c_{63}-c_{62}c_{34}c_{43}c_{56}c_{14}c_{23})}{c_{13}c_{24}c_{31}c_{42}c_{57}c_{68}-c_{14}c_{23}c_{34}c_{43}c_{56}c_{65}}$$

$$d_{41}=-\frac{c_{51}c_{14}c_{23}c_{34}c_{43}c_{65}}{c_{13}c_{24}c_{31}c_{42}c_{57}c_{68}-c_{14}c_{23}c_{34}c_{43}c_{56}c_{65}};\quad d_{42}=-\frac{c_{52}c_{14}c_{23}c_{34}c_{43}c_{65}}{c_{13}c_{24}c_{31}c_{42}c_{57}c_{68}-c_{14}c_{23}c_{34}c_{43}c_{56}c_{65}}$$

$$d_{51}=\frac{c_{51}c_{13}c_{24}c_{31}c_{42}c_{68}}{c_{13}c_{24}c_{31}c_{42}c_{57}c_{68}-c_{14}c_{23}c_{34}c_{43}c_{56}c_{65}};\quad d_{52}=\frac{c_{52}c_{13}c_{24}c_{31}c_{42}c_{68}}{c_{13}c_{24}c_{31}c_{42}c_{57}c_{68}-c_{14}c_{23}c_{34}c_{43}c_{56}c_{65}}$$

$$d_{61}=\frac{(c_{61}c_{13}c_{24}c_{31}c_{42}c_{57}-c_{21}c_{13}c_{33}c_{42}c_{55}c_{64})}{c_{13}c_{24}c_{31}c_{42}c_{57}c_{68}-c_{14}c_{23}c_{34}c_{43}c_{56}c_{65}};\quad d_{62}=\frac{(c_{62}c_{13}c_{24}c_{31}c_{42}c_{57}-c_{22}c_{13}c_{33}c_{42}c_{55}c_{64})}{c_{13}c_{24}c_{31}c_{42}c_{57}c_{68}-c_{14}c_{23}c_{34}c_{43}c_{56}c_{65}}$$

$$c_{11}=[(\kappa+1)B_1m_1-\mathrm{i}\xi(3-\kappa)]\mathrm{e}^{(m_1+\beta)h_1}\big|_{y>0};\quad c_{12}=[(\kappa+1)B_2m_2-\mathrm{i}\xi(3-\kappa)]\mathrm{e}^{(m_2+\beta)h_1}\big|_{y>0};$$

$$c_{13}=[(\kappa+1)B_3m_3-\mathrm{i}\xi(3-\kappa)]\mathrm{e}^{(m_3+\beta)h_1}\big|_{y>0};\quad c_{14}=[(\kappa+1)B_4m_4-\mathrm{i}\xi(3-\kappa)]\mathrm{e}^{(m_4+\beta)h_1}\big|_{y>0};$$

$$c_{21}=(m_1-\mathrm{i}\xi B_1)\mathrm{e}^{(m_1+\beta)h_1}\big|_{y>0};\quad c_{22}=(m_2-\mathrm{i}\xi B_2)\mathrm{e}^{(m_2+\beta)h_1}\big|_{y>0};$$

$$c_{23}=(m_3-\mathrm{i}\xi B_3)\mathrm{e}^{(m_3+\beta)h_1}\big|_{y>0};\quad c_{24}=(m_4-\mathrm{i}\xi B_4)\mathrm{e}^{(m_4+\beta)h_1}\big|_{y>0};$$

$$c_{31}=[(\kappa+1)B_1m_1-\mathrm{i}\xi(3-\kappa)]\mathrm{e}^{-(m_1+\beta)h_2}\big|_{y<0};\quad c_{32}=[(\kappa+1)B_2m_2-\mathrm{i}\xi(3-\kappa)]\mathrm{e}^{-(m_2+\beta)h_2}\big|_{y<0};$$

$$c_{31}=[(\kappa+1)B_3m_3-\mathrm{i}\xi(3-\kappa)]\mathrm{e}^{-(m_3+\beta)h_2}\big|_{y<0};\quad c_{34}=[(\kappa+1)B_4m_4-\mathrm{i}\xi(3-\kappa)]\mathrm{e}^{-(m_4+\beta)h_2}\big|_{y<0};$$

$$c_{41}=(m_1-\mathrm{i}\xi B_1)\mathrm{e}^{-(m_1+\beta)h_2}\big|_{y<0};\quad c_{42}=(m_2-\mathrm{i}\xi B_2)\mathrm{e}^{-(m_2+\beta)h_2}\big|_{y<0};$$

$$c_{43}=(m_3-\mathrm{i}\xi B_3)\mathrm{e}^{-(m_3+\beta)h_2}\big|_{y<0};\quad c_{44}=(m_4-\mathrm{i}\xi B_4)\mathrm{e}^{-(m_4+\beta)h_2}\big|_{y<0};$$

$$c_{51}=[(\kappa+1)B_1m_1-\mathrm{i}\xi(3-\kappa)]\big|_{y>0};\quad c_{52}=[(\kappa+1)B_2m_2-\mathrm{i}\xi(3-\kappa)]\big|_{y>0};$$

$$c_{53}=[(\kappa+1)B_3m_3-\mathrm{i}\xi(3-\kappa)]\big|_{y>0};\quad c_{54}=[(\kappa+1)B_4m_4-\mathrm{i}\xi(3-\kappa)]\big|_{y>0};$$

$$c_{55}=[(\kappa+1)B_1m_1-\mathrm{i}\xi(3-\kappa)]\big|_{y<0};\quad c_{56}=[(\kappa+1)B_2m_2-\mathrm{i}\xi(3-\kappa)]\big|_{y<0};$$

$$c_{57}=[(\kappa+1)B_1m_1-\mathrm{i}\xi(3-\kappa)]\big|_{y<0};\quad c_{58}=[(\kappa+1)B_4m_4-\mathrm{i}\xi(3-\kappa)]\big|_{y<0};$$

$$c_{61}=(m_1-\mathrm{i}\xi B_1)\big|_{y>0};\quad c_{62}=(m_2-\mathrm{i}\xi B_2)\big|_{y>0};\quad c_{63}=(m_3-\mathrm{i}\xi B_3)\big|_{y>0};\quad c_{64}=(m_4-\mathrm{i}\xi B_4)\big|_{y>0};$$

$$c_{65}=(m_1-\mathrm{i}\xi B_1)\big|_{y<0};\quad c_{66}=(m_2-\mathrm{i}\xi B_2)\big|_{y<0};\quad c_{67}=(m_3-\mathrm{i}\xi B_3)\big|_{y<0};\quad c_{68}=(m_4-\mathrm{i}\xi B_4)\big|_{y<0};$$

$$c_{71}=B_1\big|_{y>0};\quad c_{72}=B_2\big|_{y>0};\quad c_{73}=B_3\big|_{y>0};\quad c_{74}=B_4\big|_{y>0};$$

$$c_{75}=B_1\big|_{y<0};\quad c_{76}=B_2\big|_{y<0};\quad c_{77}=B_3\big|_{y<0};\quad c_{78}=B_4\big|_{y<0};$$

$$e_{11}=1+d_{11}+d_{21}-d_{31}-d_{41}-d_{51}-d_{61};\quad e_{12}=1+d_{12}+d_{22}-d_{32}-d_{42}-d_{52}-d_{62};$$

$$e_{21}=c_{71}+c_{73}d_{11}+c_{74}d_{21}-c_{75}d_{31}-c_{76}d_{41}-c_{77}d_{51}-c_{78}d_{61};$$

$$e_{22}=c_{72}+c_{73}d_{12}+c_{74}d_{22}-c_{75}d_{32}-c_{76}d_{42}-c_{77}d_{52}-c_{78}d_{62};$$

$$H_{11}=\mathrm{i}(c_{51}e_{22}-c_{52}e_{21}+c_{53}d_{11}e_{22}-c_{53}d_{12}e_{21}+c_{54}d_{21}e_{22}-c_{54}d_{22}e_{21})/[\xi(e_{11}e_{22}-e_{12}e_{21})];$$

$$H_{12}=\mathrm{i}(c_{52}e_{11}-c_{51}e_{12}-c_{53}d_{11}e_{12}+c_{53}d_{12}e_{11}-c_{54}d_{21}e_{12}+c_{54}d_{22}e_{11})/[\xi(e_{11}e_{22}-e_{12}e_{21})];$$

$$H_{21}=\mathrm{i}(c_{61}e_{22}-c_{62}e_{21}+c_{63}d_{11}e_{22}-c_{63}d_{12}e_{21}+c_{64}d_{21}e_{22}-c_{64}d_{22}e_{21})/[\xi(e_{11}e_{22}-e_{12}e_{21})];$$

$$H_{22}=\mathrm{i}(c_{62}e_{11}-c_{61}e_{12}-c_{63}d_{11}e_{12}+c_{63}d_{12}e_{11}-c_{64}d_{21}e_{12}+c_{64}d_{22}e_{11})/[\xi(e_{11}e_{22}-e_{12}e_{21})].$$

References

Chen, Y.F., Erdogan, F., 1996. The interface crack problem for a nonhomogeneous coating bonded to a homogeneous substrate. J. Mech. Phys. Solids 44, 771–787.

Delale, F., Erdogan, F., 1988. On the mechanical modeling of the interfacial region in bonded half-planes. J. Appl. Mech. 55, 317–324.

Erdogan, F., Gupta, G.D., 1972. On the numerical solution of singular integral equations. Quart. Appl. Math. 29 (4), 525–534.

Guo, L.C., Wu, L.Z., Zeng, T., Ma, L., 2004. The dynamic fracture behavior of a functionally graded coating–substrate system. Compos. Struct. 64, 433–441.

Huang, G.Y., Wang, Y.S., Dietmar, G., 2002. Fracture analysis of functionally graded coatings: antiplane deformation. Euro. J. Mech. A/Solids 21, 391–400.

Huang, G.Y., Wang, Y.S., Gross, D., 2003. Fracture analysis of functionally graded coating: plane deformation. Euro. J. Mech. A/Solids 22, 535–544.

Huang, G.Y., Wang, Y.S., Yu, S.W., 2004. Fracture analysis of a functionally graded interfacial zone under plane deformation. Int. J. Solids Struct. 41, 731–743.

Jin, Z.H., Batra, R.C., 1996a. Some fracture mechanics concepts in functionally graded materials. J. Mech. Phys. Solids 44 (8), 1221–1235.

Jin, Z.H., Batra, R.C., 1996b. Interface cracking between functionally graded coatings and a substrate under antiplane shear. Int. J. Eng. Sci. 34 (15), 1705–1716.

Jin, Z.H., Noda, N., 1994. Crack-tip singular fields in nonhomogeneous materials. J. Appl. Mech. 61 (3), 738–740.

Kim, J.H., Paulino, G.H., 2002. Finite element evaluation of mixed-mode stress intensity factor in functionally graded materials. Int. J. Numer. Methods Eng. 53 (8), 1903–1935.

Konda, N., Erdogan, F., 1994. The mixed mode crack problem in a nonhomogeneous elastic medium. Eng. Fract. Mech. 47, 533–545.

Li, C.Y., Weng, G.J., 2001. Dynamic stress intensity factors of a cylindrical interface crack with a functionally graded interlayer. Mech. Mater. 33, 325–333.

Lucia, D.C., Paolo, V., 2004. Finite elements for functionally graded Reissner–Mindlin plates. Comput. Methods Appl. Mech. Eng. 193, 705–725.

Miller, M.K., Guy, W.T., 1966. Numerical inversion of the Laplace transform by use of Jacobi polynomials. J. Numer. Anal. 3, 624–635.

Qian, G., Nakamura, T., Berndt, C.C., Leigh, S.H., 1997. Tensile toughness test and high temperature fracture analysis of thermal barrier coatings. Acta Mater. 45 (4), 1767–1784.

Rice, J.R., 1988. Elastic fracture mechanics concepts for interfacial cracks. J. Appl. Mech. 55, 98–103.

Shaw, L., Leon, 1998. Thermal residual stresses in plates and coatings composed of multi-layered and functionally graded materials. Composites Part B: Eng. 29 (3), 199–210.

Taher, M., Saif, A., Hui, C.Y., 1994. Plane strain asymptotic field of a crack growing along an elastic–elastic power law creeping bimaterial interface. J. Mech. Phys. Solids 42 (2), 181–214.

Tang, L.Q., Li, Y.D., Liu, C.H., 2004. Asymptotic analysis of mode II stationary growth crack on elastic–elastic power law creeping bimaterial interface. Appl. Math. Mech. 25 (2), 228–235.

Wang, T.C., 1990. Elastic–plastic asymptotic fields for cracks on bimaterial interfaces. Eng. Fract. Mech. 37 (3), 527–538.

Wang, X.Y., Zou, Z.Z., Wang, D., 1997. On the penny-shaped crack in a nonhomogeneous interlayer of adjoining two different elastic materials. Int. J. Solids Struct. 34, 3911–3921.

Wang, B.L., Mai, Y.W., Sun, Y.G., 2003a. Anti-plane fracture of a functionally graded material strip. Euro. J. Mech. A/Solids 22 (3), 357–368.

Wang, Y.S., Huang, G.Y., Gross, D., 2003b. On the mechanical modeling of functionally graded interfacial zone with a Griffith crack: anti-plane deformation. J. Appl. Mech. 70, 676–680.

Williams, M.L., 1959. The stress around a fault or crack in dissimilar media. Bull. Seismol. Soc. Am. 49 (2), 199–204.